

Nanoporosity improved water absorption, in vitro degradability, mineralization, osteoblast responses and drug release of poly(butylene succinate)-based composite scaffolds containing nanoporous magnesium silicate compared with magnesium silicate

Zhaoying Wu,¹ Quan Li,²
Yongkang Pan,¹ Yuan Yao,¹
Songchao Tang,¹ Jiacan Su,²
Jung-Woog Shin,³ Jie Wei,¹
Jun Zhao^{4,5}

¹Key Laboratory for Ultrafine Materials of Ministry of Education, East China University of Science and Technology, ²Department of Orthopaedics Trauma, Changhai Hospital, Second Military Medical University, Shanghai, People's Republic of China; ³Department of Biomedical Engineering, Inje University, Gimhae, Republic of Korea; ⁴Department of Orthodontics, ⁵Shanghai Key Laboratory of Stomatology, Shanghai Research Institute of Stomatology, Ninth People's Hospital Affiliated to Shanghai Jiao Tong University, School of Medicine, Shanghai, People's Republic of China

Correspondence: Jie Wei
East China University of Science and Technology, 130 Meilong Road, Shanghai 200237, People's Republic of China
Tel +86 21 6425 2745
Email jiewei7860@sina.com

Jun Zhao
Ninth People's Hospital Affiliated to Shanghai Jiao Tong University, 639 Zhizaoju Road, Shanghai 200011, People's Republic of China
Email yuzj_260@hotmail.com

Abstract: Bioactive composite macroporous scaffold containing nanoporosity was prepared by incorporation of nanoporous magnesium silicate (NMS) into poly(butylene succinate) (PBSu) using solvent casting–particulate leaching method. The results showed that the water absorption and in vitro degradability of NMS/PBSu composite (NMPC) scaffold significantly improved compared with magnesium silicate (MS)/PBSu composite (MPC) scaffold. In addition, the NMPC scaffold showed improved apatite mineralization ability, indicating better bioactivity, as the NMPC containing nanoporosity could induce more apatite and homogeneous apatite layer on the surfaces than MPC scaffold. The attachment and proliferation of MC3T3-E1 cells on NMPC scaffold increased significantly compared with MPC scaffold, and the alkaline phosphatase (ALP) activity of the cells on NMPC scaffold was expressed at considerably higher levels compared with MPC scaffold. Moreover, NMPC scaffold with nanoporosity not only had large drug loading (vancomycin) but also exhibited drug sustained release. The results suggested that the incorporation of NMS into PBSu could produce bioactive composite scaffold with nanoporosity, which could enhance water absorption, degradability, apatite mineralization and drug sustained release and promote cell responses.

Keywords: nanocomposite, degradability, apatite mineralization, cell behaviors, drug release

Introduction

Today, there are increasing demands for synthetic biomaterials to repair tissue/organ defects caused by trauma, infection, tumor, congenital diseases and so on.¹ The use of nanobiomaterials in bone tissue regeneration/repair has drawn significant attention in the past few years.^{2,3} In the previous investigation, the nanoporous biomaterials, such as bioglass, calcium silicate and magnesium silicate (MS), have been revealed to possess improved apatite mineralization ability, degradability and drug sustained release and exhibit promotion effects on attachment, proliferation and differentiation of osteoblasts and the formation of new bone both in vitro and in vivo.⁴⁻⁶ The large specific surface area and high pore volume of nanoporous biomaterials may improve their biological performances and allow them to be loaded with osteogenic agents and therefore promote new bone tissue regeneration.^{7,8}

The preparation and application of biocomposite containing inorganic bioactive particles and biodegradable polymeric materials for tissue regeneration have drawn significant attention in the past few years.^{9,10} Among the biodegradable polymeric materials, poly(butylene succinate) (PBSu) is a type of aliphatic polyester, one of the most commercially available degradable polymers, which is a promising candidate for tissue engineering scaffolds and tissue implantation repair applications due to its good biocompatibility.¹¹ PBSu has low melting point, excellent elongation rate at break and good processability, by which it can be processed into various molded products using conventional equipment.¹² In addition, the degradation product of PBSu is succinic acid, which is an intermediate in the biological tricarboxylic acid cycle, and PBSu could be finally degradable into carbon dioxide *in vivo*.¹³

In the past few decades, some bioactive materials containing magnesium (Mg) element have been reported, such as Mg and Mg alloys, Mg-based bioactive glasses/bioceramics/cements and coatings.^{14,15} The magnesium element has been reported to play important roles in bone remodeling and skeletal tissue development of human beings.¹⁶ Furthermore, Mg element may enhance bone tissue mineral density and influence bone fragility, and lack of Mg element will affect all stages of skeletal metabolism, causing slow growth of bone tissue and osteoporosis.¹⁷ In a previous study, Zhang et al¹⁸ prepared mesoporous calcium–MS–PBSu scaffolds and showed that the scaffolds with improved degradability and bioactivity (compared with the PBSu scaffold) stimulated osteoblast attachment and proliferation. Our previous study has shown that the mesoporous magnesium silicate (m-MS) with large surface area and high pore volume exhibited rapid degradability, good *in vitro* bioactivity and cytocompatibility.⁵ Moreover, the results indicated that incorporation of m-MS into PBSu enhanced the degradability, bioactivity and cell responses of the scaffolds *in vitro* and promoted new bone formation of the scaffolds *in vivo* as compared with PBSu scaffold.¹⁹ However, the roles and effects of nanoporosity on the properties of the composite scaffolds are not clear. Therefore, in this study, the nanoporous magnesium silicate (NMS) and MS without nanopores as the bioactive fillers were fabricated and incorporated into PBSu to prepare NMS/PBSu composite (NMPC) and MS/PBSu composite (MPC) scaffolds. The purpose of this study was to compare the properties of water absorption, *in vitro* degradability, apatite mineralization, osteoblast responses and drug release of the two kinds of composite scaffolds and uncover the

effects of nanoporosity on the performances of the NMPC scaffolds.

Materials and methods

Preparation and characterization of NMPC and MPC scaffolds

PBSu was purchased from Shanghai Showa Highpolymer Co. Ltd, and NMS and MS were synthesized according to the following procedure.²⁰ Briefly, NMS was synthesized by a modified template-induced and self-assembling method using cetyl trimethyl ammonium bromide (CTAB) as a structure-directing agent, magnesium nitrate hexahydrate as a magnesium source and tetraethyl orthosilicate as a silica source. The samples were successively centrifuged, dried and calcinated to obtain the final white powder. At the same time, MS was synthesized in the same way without adding CTAB. The nanoporous structure of NMS was confirmed by high-resolution transmission electron microscopy (HRTEM, JEM-2010; JEOL, Tokyo, Japan) and X-ray diffraction (XRD; Geigerflex; Rigaku Co. Ltd., Tokyo, Japan). Brunauer–Emmett–Teller (BET) and Barrett–Joyner–Halenda (BJH) analyses were used to determine the surface area and the pore size distribution with a Micromeritics porosimeter (Tristar 3000; Micro-metrics Instrument Corp., Norcross, GA, USA). The surface morphology of the NMS and MS was characterized by scanning electron microscopy (SEM; S-3400N; Hitachi, Tokyo, Japan). Measurement of particle size distribution was performed by dynamic light scattering (DLS) using a Nicomp™ 380 ZLS zeta-potential/particle sizer (PSS-Nicomp Particle Sizing Systems, Santa Barbara, CA, USA).

The NMPC scaffolds with NMS content of 30 wt% were prepared by solvent casting–particulate leaching method. In brief, PBSu was dissolved in dimethyl formamide at a concentration of 10% (w/v), and then NMS powder was added into the solution, followed by continuous stirring to disperse uniformly. Sodium chloride particulates (NaCl, 300–400 μm), as the porogens, were added into the NMPC slurry and stirred for 1 hour. The mixture was then cast into polytetrafluoroethylene (PTFE) molds ($\Phi 12 \times 2$ mm). The obtained samples were air-dried at 55°C for >24 hours to remove any remaining solvent. After that, the samples were immersed into water for 48 hours at 60°C to leach out the NaCl particulates, and then the samples were dried at 55°C for 12 hours to obtain the NMPC scaffolds. The MPC scaffolds with MS content of 30 wt% were prepared as a control in the same way. The surface morphology of the scaffolds was observed by SEM and energy dispersive spectroscopy (Falcon; EDAX Co., Mahwah, NJ, USA).

Porosity and water absorption of NMPC and MPC scaffolds

The porosities of the NMPC and MPC scaffolds were measured using Archimedes' principle at room temperature:²¹ Porosity (%) = $(W_2 - W_1)/(W_2 - W_3) \times 100$, where W_1 , W_2 and W_3 are the dry weight of the scaffolds, weight of the scaffolds saturated with water and the weight of the scaffolds suspended in water, respectively.

The water absorptions of the NMPC and MPC scaffolds were evaluated by measuring the weight gain after the samples were soaked in water for different times. Briefly, the samples ($\Phi 12 \times 2$ mm) were weighed and then immersed into water for 1, 2, 3, 6, 12 and 24 hours. At the predetermined time points, the specimens were removed from water, the water on the surface was wiped off and the weights of the samples were measured. The water absorption ratio of the samples at different time points was determined by the following equation:²² Water absorption (%) = $(W_t - W_0)/(W_0) \times 100$, where W_0 is the starting weight and W_t is the weight of the samples at time t .

In vitro degradation of NMPC and MPC scaffolds

The in vitro degradations of the NMPC and MPC scaffolds were evaluated by monitoring the weight loss ratio of the samples soaked in phosphate-buffered saline (PBS, pH = 7.4) for different times. Briefly, the samples were weighed to record the initial weight (W_0) and then immersed in PBS solution using a shaking water bath at 37°C. The PBS solution was replaced once a week. At different time points (1, 2, 4, 6, 8, 10 and 12 weeks), the specimens were taken out, dried at 55°C for 24 hours and followed by weighing again (W_n). The weight loss ratio of the samples at different time points was calculated as follows:²³ Weight loss ratio (%) = $(W_0 - W_n)/(W_0) \times 100$. The pH variation of the PBS solution after the samples were soaked for different times was monitored by using a pH meter (FE20, Mettler Toledo).

Mineralization of NMPC and MPC scaffolds

The mineralization of the NMPC and MPC scaffolds was carried out in a simulated body fluid (SBF), which was prepared by the method described by Kokubo and Takadama.²⁴ The scaffold samples were immersed in SBF at a solid/liquid mass ratio of 0.1 g/20 mL using a shaking water bath at 37°C. At 3 and 5 days, the specimens were removed from the given solution, washed thoroughly with

deionized water and dried at 55°C for 24 hours. The surface morphology and chemical compositions of the samples were characterized by SEM and EDS, respectively. The changes of the ion concentrations (Si, Mg, Ca and P) in SBF after the samples were soaked for different times were determined by inductively coupled plasma atomic emission spectroscopy (ICP-AES; IRIS 1000; Thermo Electron Corp., Waltham, MA, USA).

Cell culture experiments

The MC3T3-E1 cells are a well-studied pre-osteoblastic cell line derived from mouse calvaria and the commonly used model of osteogenesis in vitro.²⁵ In this study, the MC3T3-E1 murine preosteoblasts (American Type Culture Collection; Chinese Academy of Sciences, Shanghai, China) were cultured in the Dulbecco's Modified Eagle's Medium (DMEM; Gibco, Grand Island, NY, USA) with 10% (v/v) fetal calf serum (Sijiqing, Hangzhou, China) and 1% (v/v) penicillin/streptomycin at 37°C in a 100% standard humidified atmosphere with 5% CO₂. The culture medium was replaced at 3-day intervals. The 0.25% trypsin was used to digest and passage cells. The cells were resuspended in fresh culture medium before seeding on specimens in 24-well tissue culture plates. A seeding density of 4×10^4 cells/well was used for studies on attachment, proliferation and osteogenic differentiation assays. The samples of NMPC and MPC scaffolds were first rinsed with 70% alcohol solution followed by complete drying in vacuum and then sterilized with ultraviolet (UV) radiation for 1 hour.

Cell attachment

For cell attachment experiments, the MC3T3-E1 cells were seeded on the scaffolds and allowed to attach for 3, 6 and 12 hours. At the prescribed time points, the culture medium was removed. Thereafter, the residual cultured medium and unattached cells were removed by washing with PBS solution. The adherents of the cells on the scaffolds and the tissue culture plate were detached with trypsin and then analyzed using the flow cytometer FACSCalibur (BD Biosciences, Franklin Lakes, NJ, USA). The cell adhesion amount was then calculated in percent relative to the initial seeding cell number. Furthermore, after culturing for 12 hours, the samples were fixed in 2.5% glutaraldehyde overnight. Then, the samples were washed three times with PBS for 5 minutes and dehydrated by the increasing concentrations of methanol (30%, 50%, 70%, 90% and 100%). Finally, the morphology of MC3T3-E1 cells on the scaffolds was observed by SEM.

Cell proliferation assay

For the cell proliferation assay, MC3T3-E1 cells were cultured on the scaffolds in 24-well tissue culture plates up to 5 days and were determined using a Cell Counting Kit 8 (CCK-8). The empty wells containing only DMEM were used as a blank control. At each time point, the samples were gently rinsed three times with PBS to remove the unattached cells and transferred to a new 24-well plate. A total of 500 μ L DMEM containing 50 μ L CCK-8 solution (Dojindo Molecular Technologies Inc., Kumamoto, Japan) was added to each well and incubated for 3 hours. Then, 100 μ L of supernatant from each well was transferred into a 96-well plate and read at 450 nm using a microplate reader (Synergy HT; Bio-tek, Winooski, VT, USA). The mean absorbance value/optical density (OD) obtained from the blank control was subtracted from the ODs of the test groups.

Cell morphology observation

After culturing for 3 and 5 days, the samples were taken out and rinsed with PBS to remove the nonadherent cells. The adherent cells were fixed in 2.5% glutaraldehyde for 15 minutes at ambient temperature and then rinsed with PBS two times. The samples were then treated with 0.1% Triton X-100 in PBS to permeabilize the cells for 15 minutes before being incubated with 1% bovine serum albumin (BSA) in PBS for 30 minutes to block nonspecific binding sites. The cytoskeletons were labeled by incubating with fluorescein isothiocyanate (FITC; Sigma) for 30 minutes. After rinsing with PBS, the cell nuclei were contrast-labeled in blue by 4,6-diamidino-2-phenylindole dihydrochloride (DAPI; Sigma). Finally, confocal laser scanning microscopy (CLSM; Nikon A1R, Nikon Co. Ltd., Tokyo, Japan) was used to visualize the actin cytoskeletons of the cells.

Alkaline phosphatase (ALP) activity assay

The ALP activity of the cells was measured with the ALP assay in osteogenic medium at 4, 7 and 10 days. At the specific time point, the culture medium was removed from the samples and the cell lysates were obtained by adding 1 mL of 0.2% Nonidet P-40 solution (NP-40) to each well at room temperature for 1 hour. Then, 50 μ L of 1 mg/mL p-nitrophenyl phosphate (Sigma, USA) substrate solution (pH =9), containing 0.1 mol/L glycine and 0.5 mmol/L $MgCl_2$ in 1 M diethanolamine buffer, was added to each well and incubated at 37°C for 15 minutes. After that, 100 μ L of 0.1 M sodium hydroxide was added to stop the reaction, and the OD value was quantified with a microplate reader (SPECTR Amax 384; Molecular Devices, Sunnyvale, CA, USA) at a wavelength of 405 nm. The ALP activity was

expressed as the OD value per total protein amount, which was determined using the BCA protein assay kits and a series of BSA standards.

Adsorption and release of vancomycin from scaffolds

The standard curve with certain concentrations of vancomycin was measured in order to make a regression equation. Each scaffold was weighted and immersed in 10 mL of 0.5 mg/mL vancomycin hydrochloride (VH) solution to study the adsorptive property of NMPC and MPC scaffolds. The system was placed in a shaking bath with a speed of 80 rpm at 37°C and was then centrifuged to remove 200 μ L of supernatant to a 96-well plate at each soaking time (0.25, 0.5, 1, 2, 4, 8, 12, 24 and 48 hours). The OD value of supernatant was tested by enzyme-linked immunosorbent assay (ELISA, SPECTRA-max 384; Molecular Devices) at 280 nm to determine the VH concentration in PBS solution. Then the amount of loaded VH was calculated by the regression equation and recorded as the amount of loaded VH/the weight of scaffolds (mg/g).

Vancomycin release experiments were conducted by submerging vancomycin-loaded scaffolds in 10 mL of 0.01 M PBS at pH 7.4 and 37°C. The loaded amount of vancomycin in each scaffold was the same. Briefly, the vancomycin solution was added dropwise to each scaffold at a ratio: vancomycin/scaffold=0.5 mg/g, which was then dried at 37°C overnight.⁸ At pre-determined time, the PBS solution was replaced with fresh buffer media. The OD value of the solution was analyzed by ELISA again. This experiment was repeated until the release of VH by the scaffolds remained insignificant. The cumulative release amount of VH was calculated by the standard curve and recorded as the release ratio (%).²⁶

Statistical analysis

All data were analyzed with Origin 8.0 (Origin Lab Corporation, Northampton, MA, USA) and expressed as the mean \pm standard deviation ($M \pm SD$) with $n=5$. Statistical comparisons were carried out using one-way analysis of variance (ANOVA) with post hoc test.

Results

Characterization of NMS and NMPC scaffolds

Figure 1A presents the TEM images of the morphology and microstructure of the NMS. The spherical-shaped particles with the diameter of ~200 nm and a wormlike nanoporous structure can be observed. In the small-angle XRD pattern of the NMS (Figure 1B), three apparent diffraction peaks

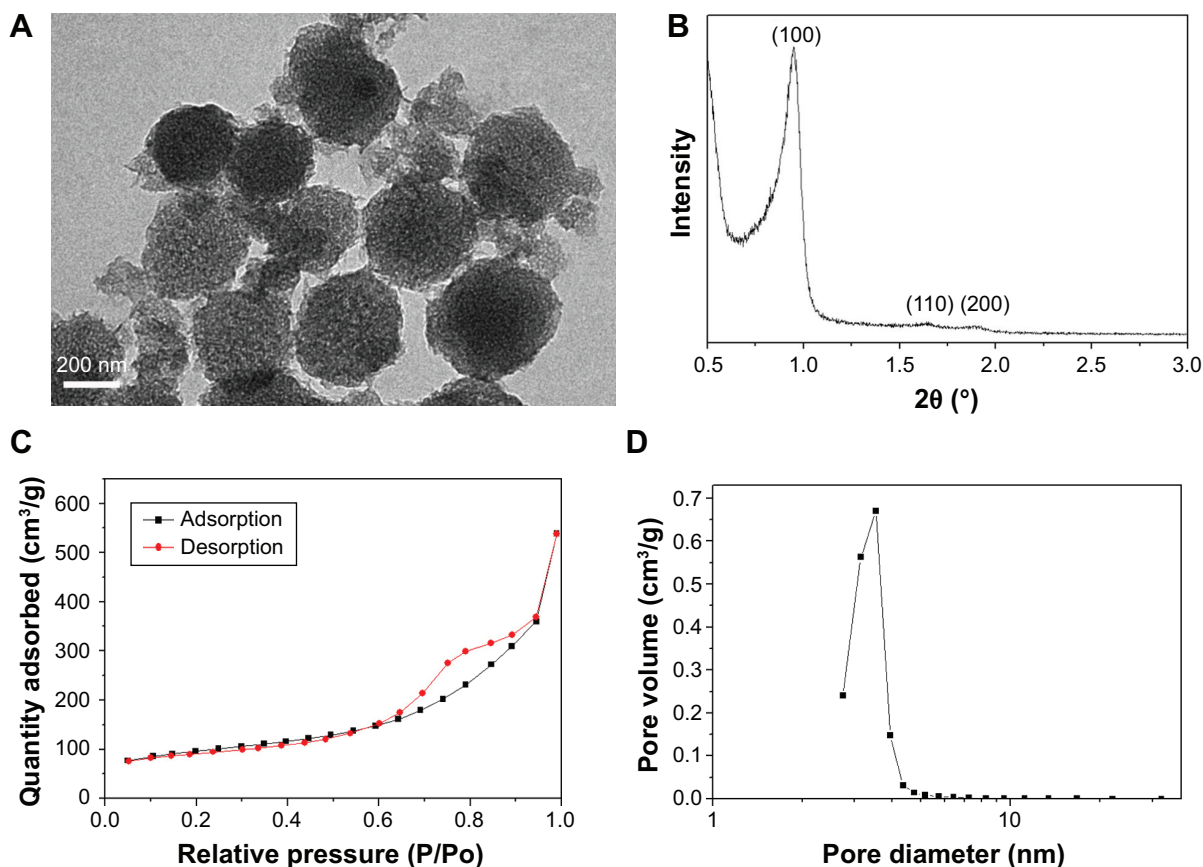


Figure 1 (A) TEM image, magnification $\times 50,000$, (B) XRD, (C) N_2 adsorption–desorption isotherms and (D) pore diameter distribution of NMS. **Abbreviations:** TEM, transmission electron microscopy; XRD, X-ray diffraction; NMS, nanoporous magnesium silicate.

could be indexed as (100), (110) and (200) reflections, which agreed with the ordered two-dimensional (2D) hexagonal mesoporous structure (p6mm), indicating nanoporous structure of NMS.²⁷

Figure 1C illustrates the N_2 adsorption–desorption isotherms of the NMS particles. The typical IV isotherms implied the characteristic of nanopores of the NMS. The result calculated from the adsorption–desorption isotherm by BJH method is shown in Figure 1D. The NMS displayed a very narrow pore size distribution with an average pore size of ~ 4 nm and a relatively large BET surface area of $538 \text{ m}^2/\text{g}$, and the single-point adsorption total pore volume at $P/P_0 = 0.989$ was $0.67 \text{ cm}^3/\text{g}$.

Figure 2 presents the SEM images of the surface morphology of the NMS and MS particles. It can be observed that the diameter of the spherical NMS particles was ~ 200 nm (Figure 2A and C). However, the size of irregular MS particles was $\sim 1 \mu\text{m}$, and some MS particles aggregated together to form bigger particles with size of several micrometers (Figure 2B and D). That was further confirmed by diameter distribution curves in Figure 2E. Using DLS, NMS showed a narrow particle size distribution around 200 nm.

However, the average size of MS, with a relative broad size distribution, was $\sim 1 \mu\text{m}$ (1,000 nm). The XRD patterns of both NMS and MS in Figure 2F exhibited a broad reflection at $2\theta = 15^\circ\text{--}35^\circ$, indicating that the main component was an amorphous material.

Figure 3 presents the SEM images of the surface morphology of the NMPC and MPC scaffolds. It is found that the macropore size of the scaffolds is $\sim 400 \mu\text{m}$, and no obvious difference was found for both the NMPC and MPC scaffolds (Figure 3A and B). However, from higher magnification images (Figure 3C and D), many obvious MS particles with the size of $\sim 1 \mu\text{m}$ were found on the walls of macropores of MPC scaffolds, while no obvious NMS particles were found on the surface of NMPC scaffolds. The EDS shows that the C, O, Mg and Si peaks were detected in both NMPC (Figure 3E) and MPC (Figure 3F) scaffolds, confirming the incorporation of NMS and MS into PBSu.

Porosity, water absorption and degradation in vitro

Figure 4A shows the porosity of the NMPC and MPC scaffolds, and the porosity of NMPC and MPC scaffolds was

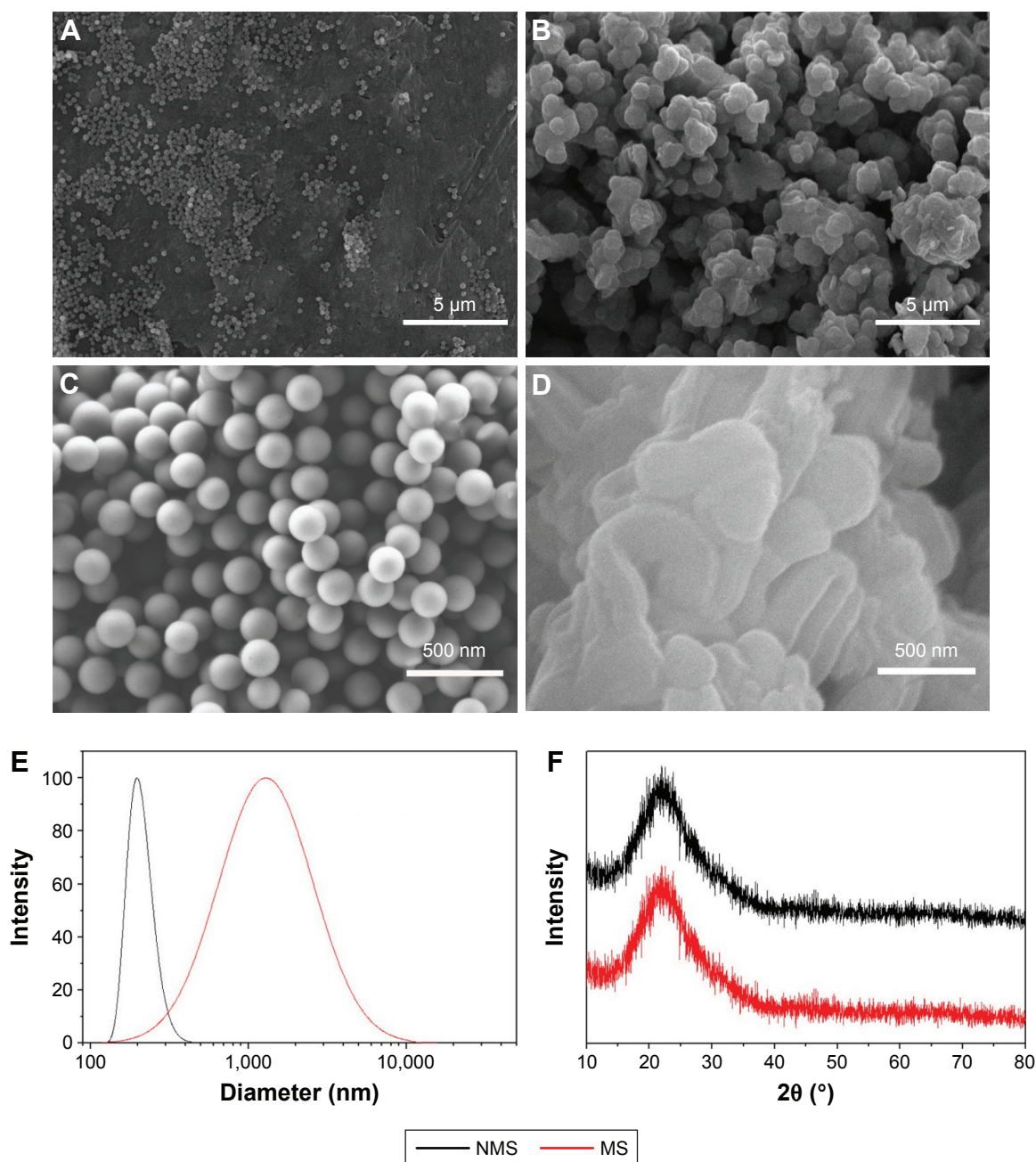


Figure 2 (A–D) SEM image of surface morphology, **(E)** diameter distribution curves and **(F)** XRD of **(A, C)** NMS and **(B, D)** MS. Magnification for **(A)** and **(B)** is $\times 3,000$; magnification for **(C)** and **(D)** is $\times 40,000$.

Abbreviations: SEM, scanning electron microscopy; XRD, X-ray diffraction; NMS, nanoporous magnesium silicate; MS, magnesium silicate.

75.3% and 60.7%, respectively. Figure 4B shows the water absorption of the NMPC and MPC scaffolds after immersion in water for 1, 2, 3, 6, 12 and 24 hours. It is found that the water absorption ratio of NMPC and MPC scaffolds was 125% and 85% at the first hour, respectively. With the increasing time, the water absorption ratio of both scaffolds increased, and the water absorption ratio of NMPC scaffolds was 237%, while the MPC scaffolds were 170% after immersion in water for 24 hours, respectively. The results

showed that water absorption ratio of the NMPC scaffolds was significantly higher than MPC scaffolds.

The weight loss ratio of the NMPC and MPC scaffolds after immersion in PBS are presented in Figure 4C. It is found that the weight loss ratios of both scaffolds increased with the incubation time, and the weight loss of the NMPC scaffolds was ~ 66 wt% at the end of 12 weeks, which was obviously higher than MPC scaffolds of 46 wt%. During the period, the pH variation of PBS solution containing the scaffolds for different

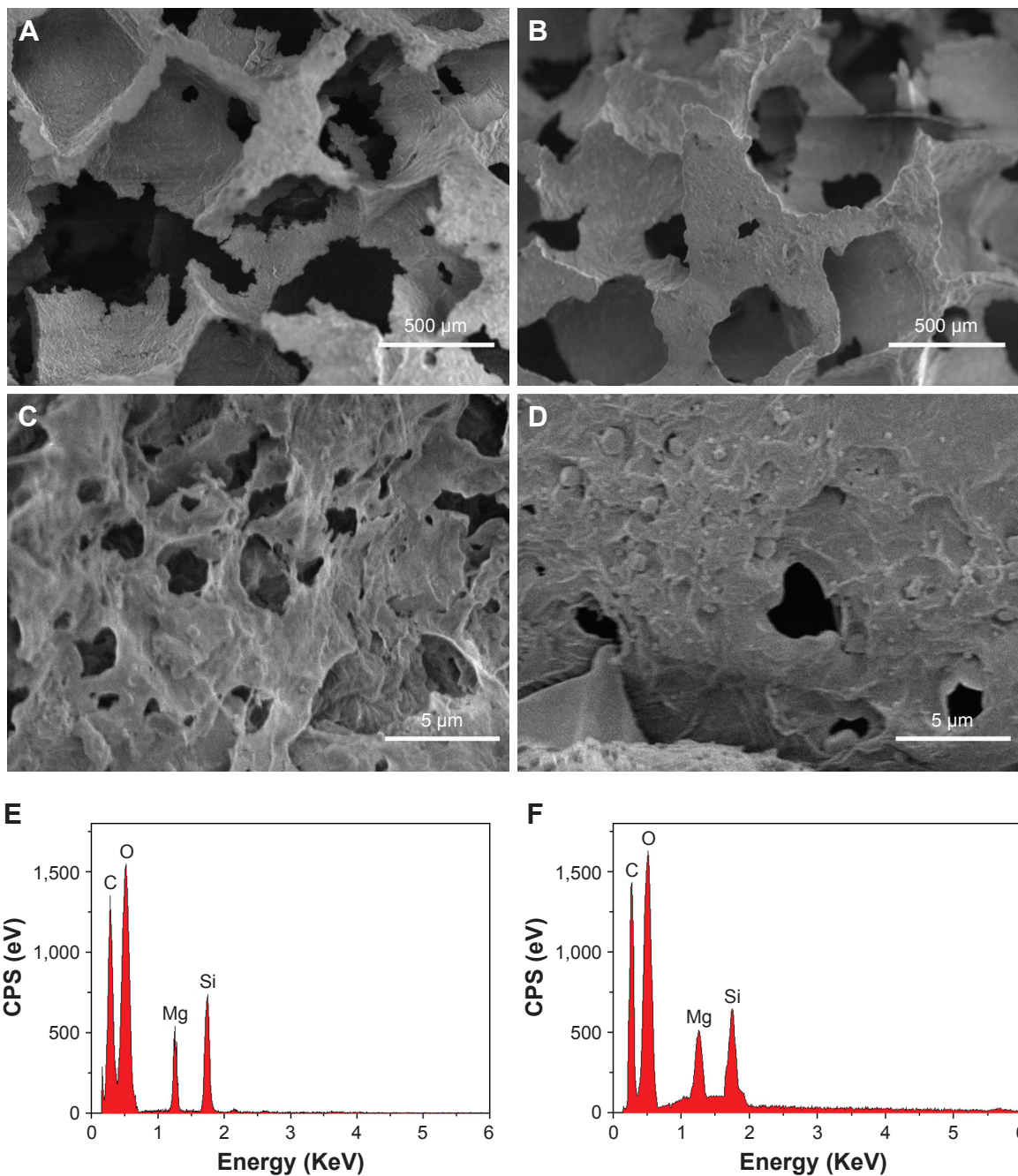


Figure 3 (A–D) SEM images of surface morphology and **(E, F)** EDS of **(A, C, E)** NMPC and **(B, D, F)** MPC scaffolds. Magnification for **(A)** and **(B)** is $\times 50$; magnification for **(C)** and **(D)** is $\times 5,000$.

Abbreviations: SEM, scanning electron microscopy; EDS, energy dispersive spectroscopy; NMS, nanoporous magnesium silicate; PBSu, poly(butylene succinate); NMPC, NMS/PBSu composite; MS, magnesium silicate; MPC, MS/PBSu composite; CPS, counts per second.

periods of time is shown in Figure 4D. The pH of the solution containing the NMPC and MPC scaffolds increased from 7.4 to 7.61 and 7.52 in the first 3 days and then slightly decreased to 7.37 and 7.31 after 28 days of immersion, respectively.

In vitro mineralization

Figure 5 exhibits the surface morphologies of the NMPC and MPC scaffolds under SEM after immersion into SBF

for 3 and 5 days. At 3 days, many vermiform granules were found on the surfaces of both the NMPC and MPC scaffolds, while some granules on the NMPC scaffold surfaces agglomerated to form spherical-shaped apatite granules. At 5 days, the surface of NMPC scaffolds was almost completely covered by numerous agglomerates of spherical-shaped particles. However, the precipitation partially covered on the MPC scaffolds with part of the surface was still smooth.

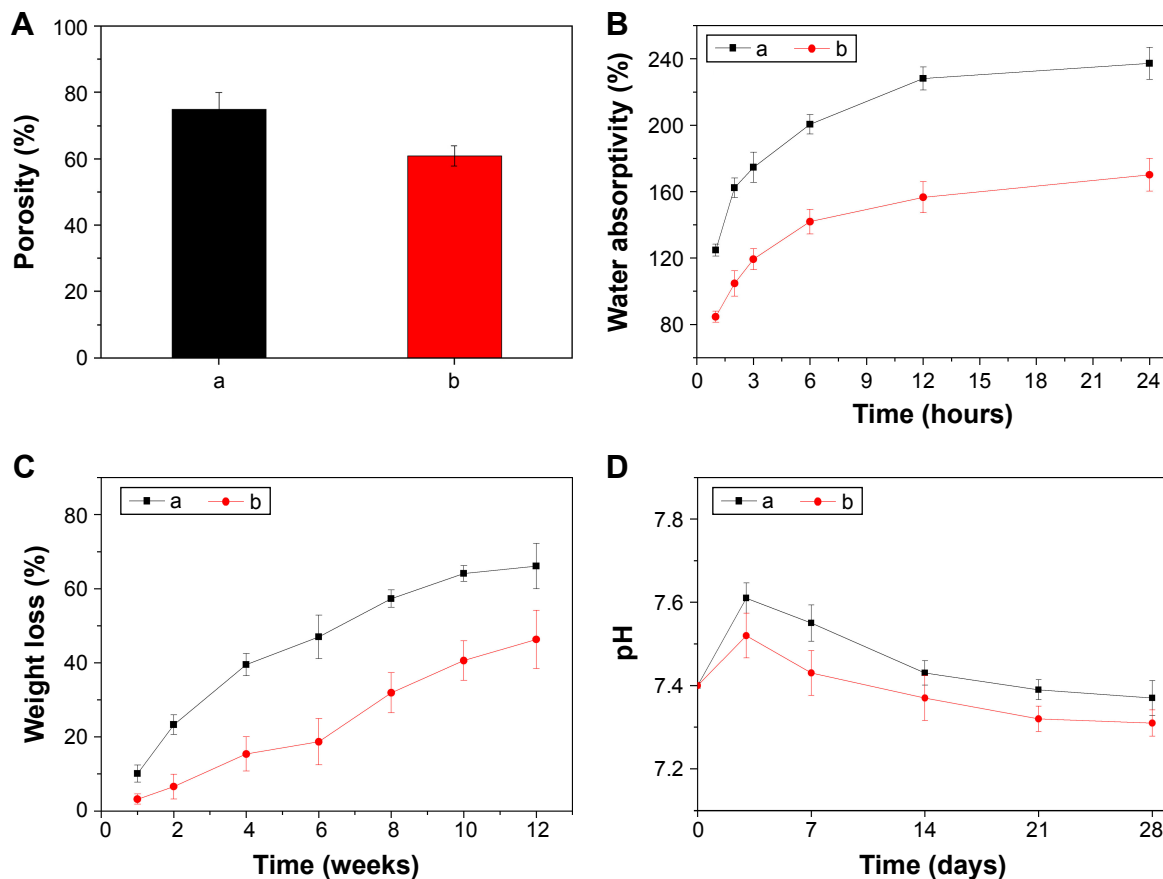


Figure 4 (A) Porosity, (B) changes of water absorption, (C) weight loss of (a) NMPC and (b) MPC scaffolds, (D) changes of pH of solution after (a) NMPC and (b) MPC scaffolds soaking in PBS with time.

Abbreviations: NMS, nanoporous magnesium silicate; PBSu, poly(butylene succinate); NMPC, NMS/PBSu composite; MS, magnesium silicate; MPC, MS/PBSu composite; PBS, phosphate-buffered saline.

The results indicated that both the NMPC and MPC scaffolds could induce apatite layers on their surfaces, while the NMPC scaffolds could induce more apatite on their surface than MPC scaffolds.

The EDS acquired from NMPC and MPC scaffold surfaces after soaking in SBF for 5 days is shown in Figure 6. It is found that both calcium and phosphorous peaks were detected, and the Ca/P mol ratios of NMPC and MPC scaffolds were 1.61 and 1.53, respectively. The results indicated that the Ca/P ratio of the formed apatite on NMPC was higher than MPC scaffolds, which was approximate to that of bone mineral of hydroxyapatite (1.67). The EDS results further confirmed the newly formed apatite on the surface of the scaffolds.

Figure 7 shows the changes of ion concentration of Ca, P, Mg and Si in solution with time after the scaffolds were soaked in SBF. It was found that the Ca and P ion concentrations in SBF for NMPC scaffolds exhibited a much faster reduction than MPC scaffolds within the first 2 days and then decreased gradually up to 5 days. In other words,

the decrease of Ca and P ion concentrations for NMPC was obviously faster than MPC scaffolds. In contrast, the Si ion concentrations in SBF for NMPC increased gradually throughout the soaking period, which was much faster than MPC scaffolds. In addition, the Mg ion concentrations in SBF increased rapidly for first 2 days and thereafter decreased at a slower rate up to 5 days.

In vitro cytocompatibility

Cell attachment

Cell attachment was assessed using MC3T3-E1 cells cultured on the NMPC and MPC scaffolds. The results of cell attachment efficiency are profiled in Figure 8A. The quantitative evaluation revealed a significant increase of adherent cells on NMPC scaffolds in comparing with MPC scaffolds at any culture time, suggesting that the NMPC scaffolds containing NMS facilitated cell adhesion.

The cell morphology on the scaffolds at different times is illustrated in Figure 8B. It was found that the

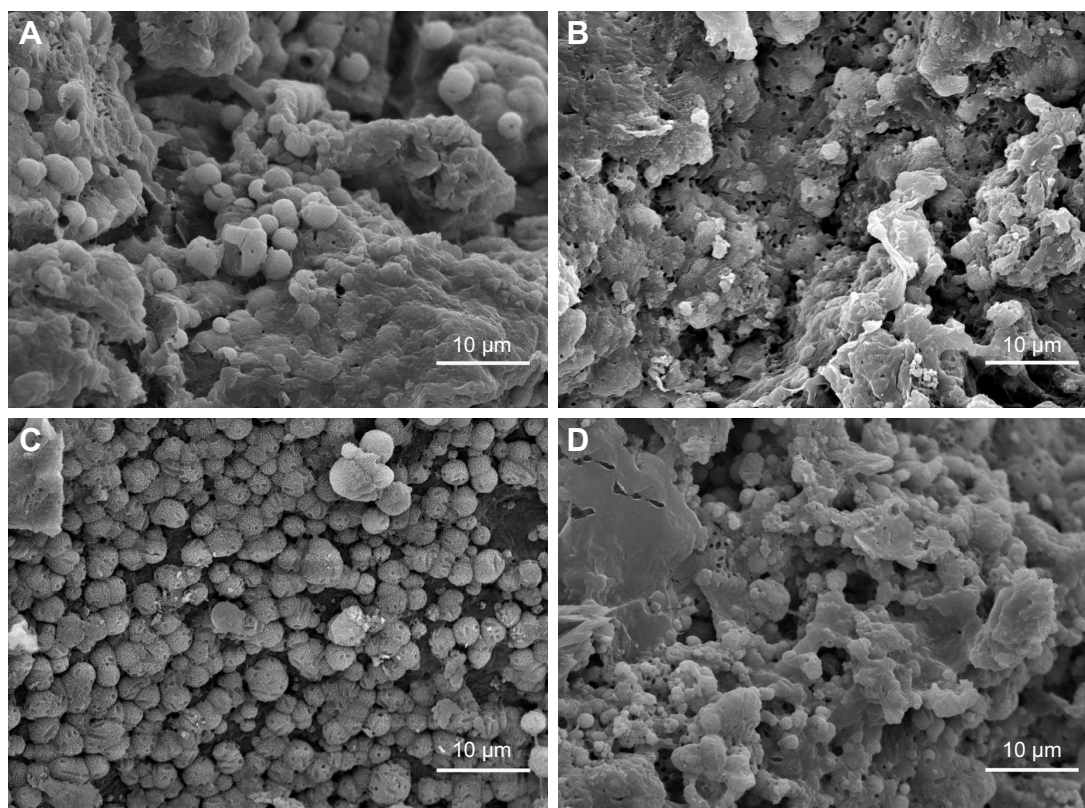


Figure 5 SEM images of surface morphology of (A, C) NMPC and (B, D) MPC scaffolds after soaking in SBF for (A, B) 3 and (C, D) 5 days. Magnification $\times 2,000$.

Abbreviations: SEM, scanning electron microscopy; NMS, nanoporous magnesium silicate; PBSu, poly(butylene succinate); NMPC, NMS/PBSu composite; MS, magnesium silicate; MPC, MS/PBSu composite; SBF, simulated body fluid.

osteoblasts stretched out and spread well on the surface of the NMPC and MPC scaffolds at 12 hours. The osteoblasts were completely spread across the macropores of scaffolds. The results indicated that both the NMPC and MPC scaffolds had no negative effects on cell morphology and viability.

Cell proliferation and cell morphology

Proliferation of MC3T3-E1 cells cultured on the NMPC and MPC scaffolds at 1, 3 and 5 days is shown in Figure 9. It is found that the OD values for both NMPC and MPC scaffolds increased with time, indicating good cytocompatibility. At 1 and 3 days, there was no obvious difference of OD value for

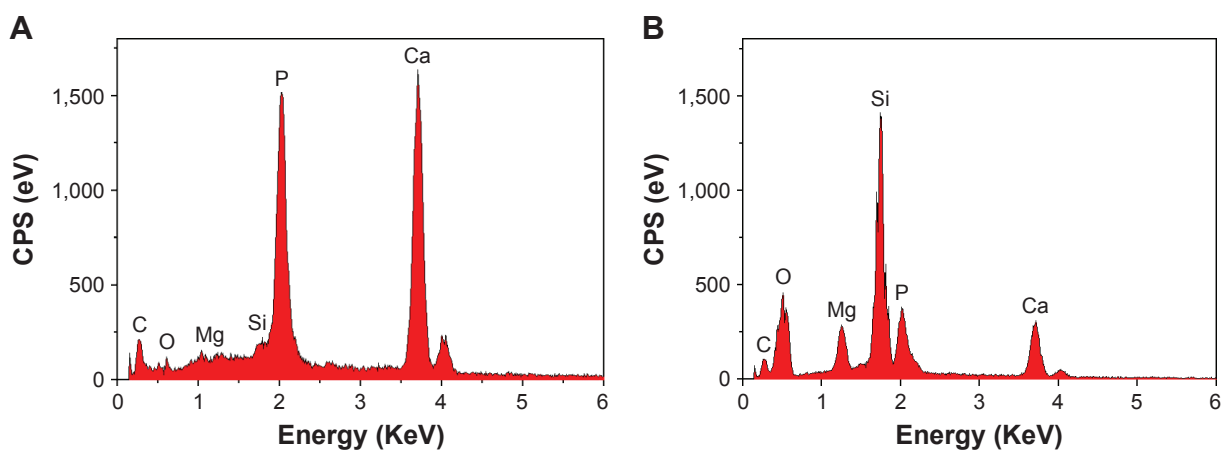


Figure 6 EDS of (A) NMPC and (B) MPC scaffolds after soaking in SBF for 5 days.

Abbreviations: EDS, energy dispersive spectroscopy; NMS, nanoporous magnesium silicate; PBSu, poly(butylene succinate); NMPC, NMS/PBSu composite; MS, magnesium silicate; MPC, MS/PBSu composite; SBF, simulated body fluid; CPS, counts per second.

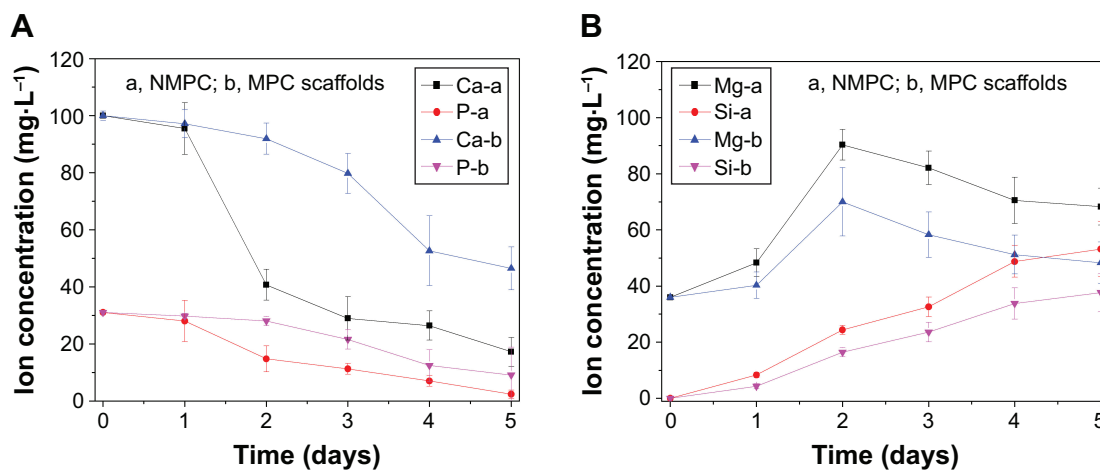


Figure 7 Changes of ion concentrations in solution after (A) NMPC and (B) MPC scaffolds immersed in SBF for different time periods.

Abbreviations: NMS, nanoporous magnesium silicate; PBSu, poly(butylene succinate); NMPC, NMS/PBSu composite; MS, magnesium silicate; MPC, MS/PBSu composite; SBF, simulated body fluid.

both NMPC and MPC scaffolds. However, the OD value for the NMPC scaffold was significantly higher than MPC scaffolds at 5 days, indicating that the proliferation of MC3T3-E1 cells on NMPC scaffolds was higher than MPC scaffolds.

The cell morphology on the scaffolds for different times is illustrated in Figure 10. It was apparent that osteoblasts on the NMPC scaffolds were spread well along the walls of macropores at 3 days, while the cells on the MPC

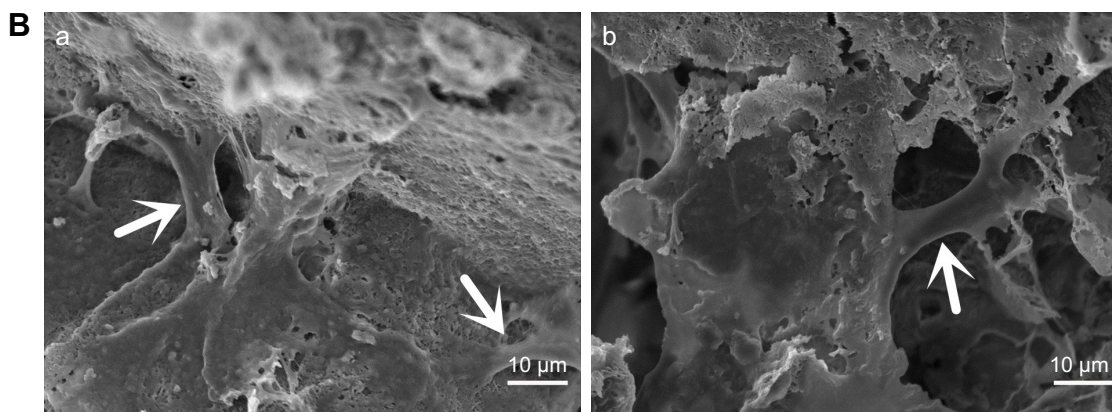
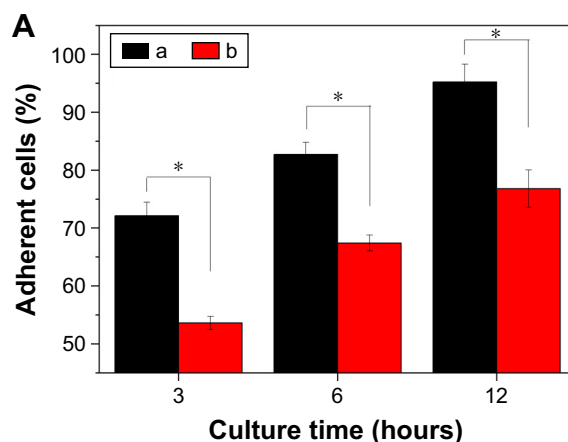


Figure 8 (A) Cell adherent percent and **(B)** SEM images of cell morphology after MC3T3-E1 cells seeding on (a) NMPC and (b) MPC scaffolds for 12 hours (the white arrows represent the cells). **P*<0.05.

Abbreviations: SEM, scanning electron microscopy; NMS, nanoporous magnesium silicate; PBSu, poly(butylene succinate); NMPC, NMS/PBSu composite; MS, magnesium silicate; MPC, MS/PBSu composite.

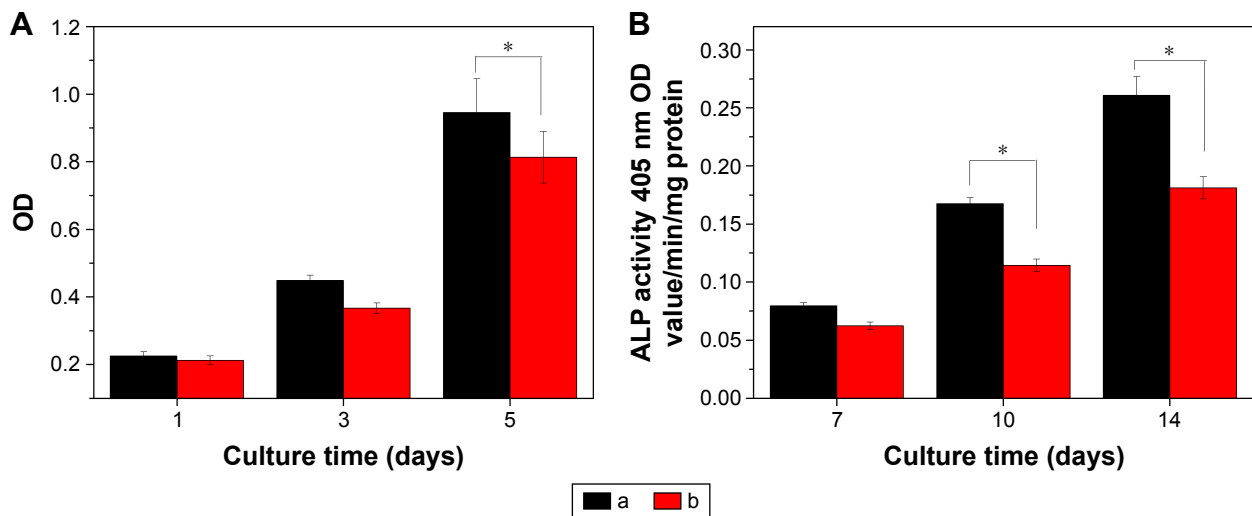


Figure 9 (A) Proliferation and (B) ALP activity of MC3T3-E1 cells cultivated on (a) NMPC and (b) MPC scaffolds. * $P < 0.05$.

Abbreviations: ALP, alkaline phosphatase; NMS, nanoporous magnesium silicate; PBSu, poly(butylene succinate); NMPC, NMS/PBSu composite; MS, magnesium silicate; MPC, MS/PBSu composite; OD, optical density.

scaffolds were almost spindle-shaped (Figure 10A and B). At 5 days, the cells penetrated deeper into the scaffolds. MC3T3-E1 with a healthy spindle shape on the surface of NMPC scaffolds attached and spread more than MPC scaffolds (Figure 10C and D). The results indicated that the NMPC scaffolds significantly promoted MC3T3-E1 cell

viability as compared with MPC scaffolds, in accordance with previous results.

ALP activity

As shown in Figure 9B, the ALP activity of MC3T3-E1 cells cultivated on both NMPC and MPC scaffolds increased

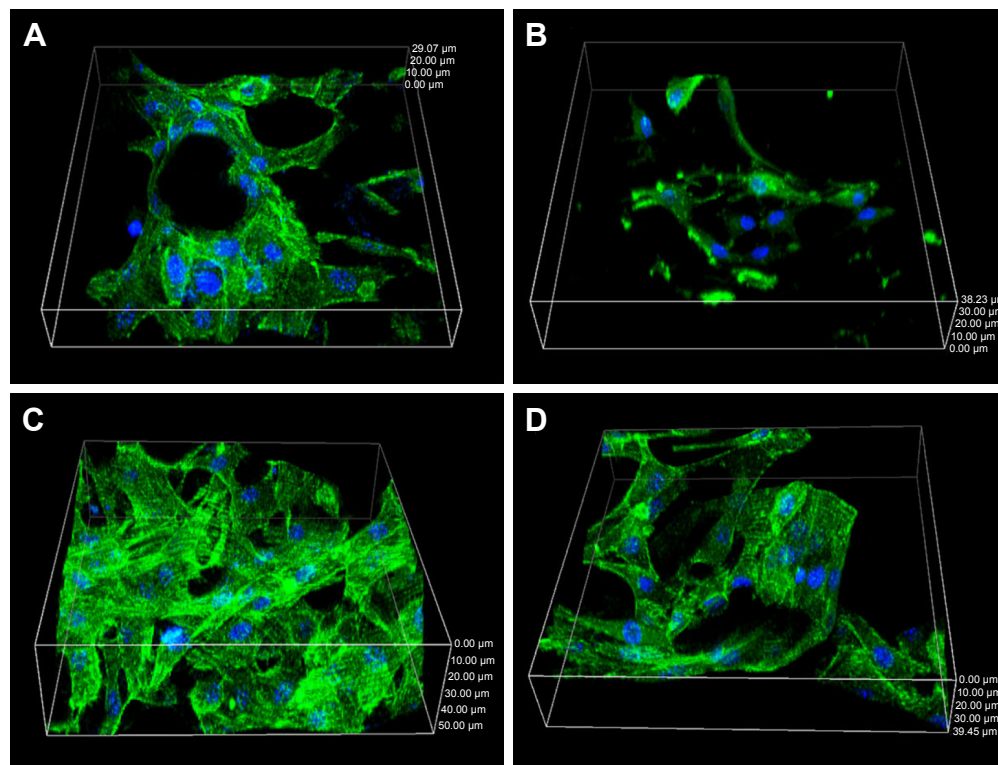


Figure 10 Morphology of MC3T3-E1 cells cultivated on (A, C) NMPC and (B, D) MPC scaffolds for (A, B) 3 and (C, D) 5 days.

Abbreviations: NMS, nanoporous magnesium silicate; PBSu, poly(butylene succinate); NMPC, NMS/PBSu composite; MS, magnesium silicate; MPC, MS/PBSu composite.

with time. It could be observed that the ALP activity of cells was expressed at low levels at 4 days, and no significant differences were detected between the NMPC and MPC scaffolds, while the ALP activity of the cells on the NMPC scaffolds was significantly higher than MPC scaffolds at 7 and 10 days, indicating that the MC3T3-E1 cells obviously differentiated. The results revealed that the NMPC scaffolds could trigger an upregulation of ALP activity as compared with MPC scaffolds.

Vancomycin loaded and release from scaffolds

Figure 11A showed the amount of vancomycin loaded in scaffolds. It could be found that the initial adsorption (at 0.25 hour) was 4 mg/g for NMPC while 0.6 mg/g for MPC scaffolds, indicating that NMPC showed more effective adsorption than MPC. At 12 hours, the NMPC was still adsorbing vancomycin until 10 mg/g at 48 hours, while the amount of vancomycin loaded in MPC reached 5.6 mg/g and stayed suspended.

The characteristics of vancomycin release from both NMPC and MPC scaffolds are summarized in Figure 11B. A burst release in the early stage was observed from MPC scaffolds followed by continuous release. At first 6 hours, the ratio of vancomycin release from MPC scaffolds was almost 58.2% while that from NMPC scaffolds was only 18.4%. The continuous release of vancomycin from NMPC scaffolds lasted until 240 hours, and the cumulative ratio of vancomycin release was 87.4%. The result indicated that the NMPC scaffolds showed lower release ratios than that of MPC scaffolds within 10 days.

Discussion

Over the past few years, composites containing biodegradable polymers and bioactive materials, such as hydroxyapatite, tricalcium phosphate, calcium silicate and bioglass, have attracted increasing attention as the promising biomaterials for bone tissue regeneration.^{28,29} In this study, the spherical-shaped NMS particles with the size of ~200 nm and irregular MS particles with the size of ~1 μm (some MS particles aggregated together to form more bigger particles with size of several micrometers) were fabricated, and the NMS and MS as bioactive materials were incorporated into PBSu matrix to form bioactive composite scaffolds by solvent casting-particulate leaching method. The results showed that both the NMS and MS particles dispersed into polymer phases, and no obvious NMS particles were found on the surface of macroporous NMPC scaffold, while some obvious particles with the size of ~1 μm were found on the surface of MPC scaffold. It can be indicated that the introduction of NMS and MS into PBSu remarkably alters the surface morphology of the two kinds of composite scaffolds.

In addition, the results revealed that both the NMPC and MPC scaffolds had the macropore with the size of ~400 μm . The porosity of the NMPC (75.3%) was obviously higher than that of the MPC scaffolds (60.7%) because the NMPC contained not only macroporosity (caused by NaCl particles) but also nanoporosity (caused by NMS), while the MPC scaffolds only contained macroporosity. Moreover, the water absorption ratio of NMPC was significantly higher than MPC scaffolds because of the presence of nanoporosity in NMPC as compared with MPC scaffolds. The containing nanoporosity and improvement of the water absorption of NMPC

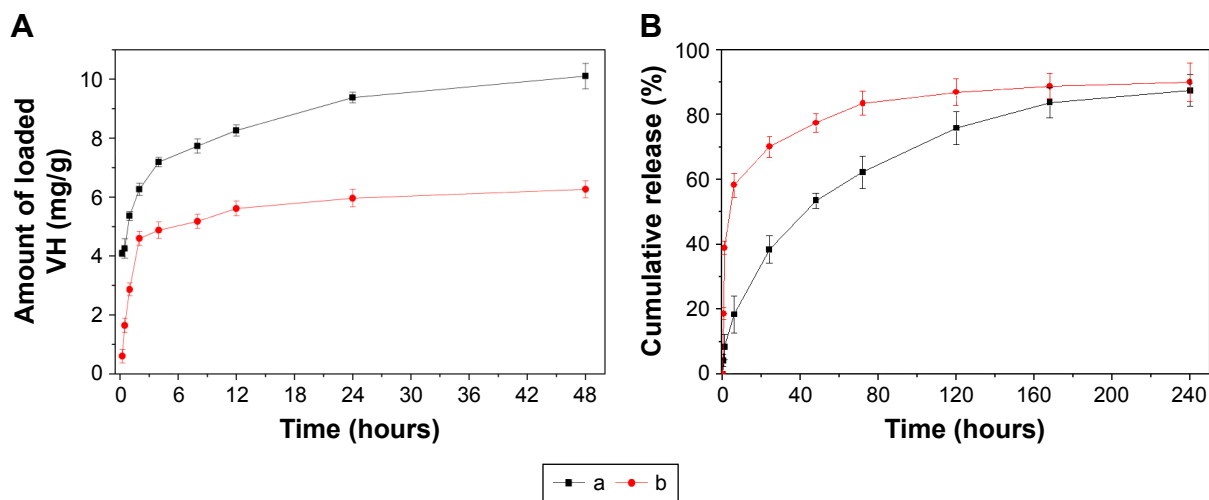


Figure 11 (A) Adsorption ability and (B) release of vancomycin by (a) NMPC and (b) MPC scaffolds.

Abbreviations: NMS, nanoporous magnesium silicate; PBSu, poly(butylene succinate); NMPC, NMS/PBSu composite; MS, magnesium silicate; MPC, MS/PBSu composite; VH, vancomycin hydrochloride.

scaffolds might be beneficial to the interactions between biomaterials and cells.

Generally, the degradation rate of bone implants should be coincident with the growth of new bone tissue and gradually replaced by new bone tissue *in vivo*.³⁰ In this study, it was found that the weight loss ratio of the NMPC scaffolds was 66 wt% after immersion in PBS for 12 weeks, which was significantly higher than MPC scaffolds of 46 wt%. The results showed that the degradation rate of the NMPC scaffolds was faster than MPC scaffolds, indicating that addition of NMS into PBSu obviously improved the degradability of the composite scaffolds as compared with MS. It could be suggested that the NMS with high surface area (538 m²/g) and pore volume (0.67 cm³/g) in PBSu increased the porosity and surface area of the composite scaffolds, which leads to more water being absorbed in the composite scaffolds, thus improving degradation of the NMPC scaffolds as compared with MPC scaffolds.

Bioactive materials can biochemically bond to bone tissue through the apatite layer formed on their surfaces *in vivo*, and the apatite layer on the implant surface plays the key roles in the formation of the bone tissue–material interface.³⁰ The *in vitro* apatite mineralization on the biomaterial surfaces in SBF could predict the *in vivo* bone bioactivity of the implants.³¹ In this study, the apatite mineralization obviously occurred on the surfaces of both the NMPC and MPC scaffolds, and the apatite formation ability for NMPC was better than MPC scaffolds, indicating that incorporation of NMS into PBSu significantly enhanced the bioactivity of NMPC as compared with MS. The results suggested that the NMPC scaffolds containing macroporosity and nanoporosity greatly accelerated the apatite mineralization and therefore enhanced the bioactivity of the NMPC scaffolds as compared with MS in PBSu. Therefore, the NMS with high specific surface area and pore volume in PBSu might play the key roles for improvement of apatite formation.

The dissolution of the NMS and MS from the NMPC and MPC scaffolds increased the local Si and Mg ion concentrations, which caused subsequent apatite mineralization.³² According to the mechanism of apatite formation on bioactive inorganic materials, it can be suggested that the processes of apatite mineralization on both the NMPC and MPC scaffolds were dependent on the dissolution velocity and ion deposition rate on the material surfaces. Moreover, the NMS with high surface area and pore volume leads to a faster release of Si and Mg ions from the NMPC than MPC scaffolds, which promoted the apatite mineralization on NMPC compared with MPC scaffolds.

In this study, the adhesion and proliferation of the MC3T3-E1 cells on the NMPC and MPC scaffolds increased with time, indicating good cytocompatibility. Moreover, the adhesion of cells on the NMPC was better than MPC scaffolds, and the proliferation of the cells on the NMPC was significantly higher than MPC scaffolds, revealing that the NMPC promoted cell adhesion and proliferation compared with MPC scaffolds. The cytoskeletal morphology of the MC3T3-E1 cells cultured on both the NMPC and MPC scaffolds was visualized using a CLSM. Generally speaking, the cells will undergo their morphological changes to stabilize the cell–material interface after contacting biomaterials.³³ It was found that the MC3T3-E1 cells could attach and grow into the NMPC and MPC scaffolds. Moreover, the number of cells in the NMPC scaffolds was significantly higher than MPC scaffolds, suggesting that the NMPC scaffolds containing NMS obviously promoted cell adhesion, proliferation and ingrowth as compared to MPC scaffolds with MS.

The osteogenic differentiation activity of cells to the biointerfaces, as far as bone-repair biomaterials concerned, is a key event in bone formation.³⁴ In this study, the ALP activity of the MC3T3-E1 cells on the NMPC scaffolds was significantly higher than MPC scaffolds, revealing that the NMPC scaffolds containing NMS obviously promoted cell differentiation as compared to MPC scaffolds containing MS. The cellular responses such as cell adhesion, proliferation and differentiation are significantly influenced by the surface characteristics of the implants such as surface morphology and chemical composition.³⁵ Compared with the MPC scaffolds, the NMPC scaffolds contained not only macroporosity but also nanoporosity, which might have significant effects on cell adhesion at early stage. In addition, homogeneous apatite layer on the NMPC scaffolds might play important roles for cell proliferation and differentiation at later stage of cell culture.

Previous studies have shown that ionic products (Si and Mg) dissolution from bioactive glasses could stimulate osteoblast proliferation.¹⁹ In addition, it was reported that sol–gel bioglass had significant osteogenic effects by releasing a proper level of Si and Mg on osteoblast-like cells.³⁶ In this study, it was found that the Si and Mg ions were continuously released from both the NMPC and MPC scaffolds into SBF, and the release rate of Si and Mg ions from the NMPC was significantly faster than MPC scaffolds. In addition, the results showed that the MC3T3-E1 cells proliferated and differentiated more quickly after being cultured on the NMPC scaffolds than MPC scaffolds. Therefore, it can be suggested that the continuous dissolution of the composite scaffolds

produced a microenvironment with rich Si and Mg ions that might be responsible for stimulating cell responses such as proliferation and differentiation. Moreover, the faster release of Si and Mg ions from NMPC scaffolds significantly promoted the cell responses as compared with MPC scaffolds.

The risk of bone infection is a serious problem associated with bone filling and replacement.³⁷ Among current pharmaceuticals, the classical antibiotic vancomycin has been widely used in the therapeutic treatment for osteomyelitis.³⁸ However, some drawbacks exist in the traditional therapy (such as injections and oral administration).³⁹ In the study, the amount of vancomycin loaded into NMPC was almost two times more than MPC scaffolds because NMPC scaffolds had not only macroporosity but also nanoporosity, which could load high amount of vancomycin into the NMPC compared with MPC scaffolds. In addition, the vancomycin could release continuously from the scaffolds, and the two scaffolds with the same amount of drugs showed distinguishing behaviors of drug release. A burst release of vancomycin at the early stage was observed in the MPC scaffolds because most of the drug was absorbed on wall surface of macropores of the scaffolds. However, NMPC scaffolds showed a slow release of vancomycin because most of the drug was absorbed into nanopores of the scaffolds. It can be suggested that the nanoporosity in the NMPC scaffolds played important roles for the gradual release of vancomycin. Therefore, the prepared NMPC scaffolds can be used to promote bone regeneration and simultaneously treat bone-related diseases, including osteomyelitis.

Conclusion

Bioactive NMPC scaffolds with macropores of ~400 μm were fabricated by adding NMS into PBSu through solvent casting–particulate leaching method. Compared with the macroporous MPC scaffolds containing MS, NMPC scaffolds with NMS contained not only macroporosity but also nanoporosity. The NMPC scaffolds containing nanoporosity could obviously enhance the water absorption, in vitro degradability and apatite mineralization ability of the composite scaffolds. In addition, the NMPC scaffolds containing nanoporosity could stimulate MC3T3-E1 cell response, such as cell attachment, proliferation and differentiation, as compared with MPC scaffolds. Furthermore, NMPC scaffolds with nanoporosity could load more drugs (vancomycin) and exhibited drug sustained release behaviors as compared with MPC scaffolds. In short, the incorporation of NMS into PBSu was a useful approach to obtain bioactive composite scaffolds with improved properties and multifunction (implanted

scaffold and drug delivery), which might be used as bone implants for repair of bone defects and drug treatment of disease (infection or tumor, etc.).

Acknowledgments

The grants were from the Major International Joint Research Project between China and Korea (81461148033), the National Research Foundation of Korea (NRF) Grant (NRF-2014K2A2A7066637) and the National Natural Science Foundation of China (51502340, 81200815 and 81271705).

Disclosure

The authors report no conflicts of interest in this work.

References

1. Chen FM, Liu X. Advancing biomaterials of human origin for tissue engineering. *Prog Polym Sci*. 2016;53:86–168.
2. Ilie I, Ilie R, Mocan T, Bartos D, Mocan L. Influence of nanomaterials on stem cell differentiation: designing an appropriate nanobiointerface. *Int J Nanomedicine*. 2012;7:2211–2225.
3. Gong T, Xie J, Liao J, Zhang T, Lin S, Lin Y. Nanomaterials and bone regeneration. *Bone Res*. 2015;3:15029.
4. Song W, Li X, Qian J, et al. Mesoporous calcium-silicon xerogels with mesopore size and pore volume influence hMSC behaviors by load and sustained release of rhBMP-2. *Int J Nanomedicine*. 2015;10:1715–1726.
5. Wu Z, Tang T, Guo H, et al. In vitro degradability, bioactivity and cell responses to mesoporous magnesium silicate for the induction of bone regeneration. *Colloids Surf B Biointerfaces*. 2014;120:38–46.
6. Zheng K, Lu M, Liu Y, et al. Monodispersed lysozyme-functionalized bioactive glass nanoparticles with antibacterial and anticancer activities. *Biomed Mater*. 2016;11(3):035012.
7. Li F, Wu W, Xiang L, et al. Sustained release of VH and rhBMP-2 from nanoporous magnesium-zinc-silicon xerogels for osteomyelitis treatment and bone repair. *Int J Nanomedicine*. 2015;10:4071–4080.
8. Tang W, Lin D, Yu Y, et al. Bioinspired trimodal macro/micro/nanoporous scaffolds loading rhBMP-2 for complete regeneration of critical size bone defect. *Acta Biomater*. 2016;32:309–323.
9. Liu T, Ding X, Lai D, et al. Enhancing in vitro bioactivity and in vivo osteogenesis of organic-inorganic nanofibrous biocomposites with novel bioceramics. *J Mater Chem B*. 2014;2(37):6293–6305.
10. Sun F, Zhou H, Lee J. Various preparation methods of highly porous hydroxyapatite/polymer nanoscale biocomposites for bone regeneration. *Acta Biomater*. 2011;7(11):3813–3828.
11. Nerantzaki M, Filippousi M, Van Tendeloo G, et al. Novel poly(butylene succinate) nanocomposites containing strontium hydroxyapatite nanorods with enhanced osteoconductivity for tissue engineering applications. *Express Polym Lett*. 2015;9(9):773–789.
12. Coutinho DF, Gomes ME, Neves NM, Reis RL. Development of micropatterned surfaces of poly(butylene succinate) by micromolding for guided tissue engineering. *Acta Biomater*. 2012;8(4):1490–1497.
13. Costa-Pinto AR, Martins AM, Castelhana-Carlos MJ, et al. In vitro degradation and in vivo biocompatibility of chitosan-poly(butylene succinate) fiber mesh scaffolds. *J Bioact Compat Polym*. 2014;29(2):137–151.
14. Han P, Cheng P, Zhang S, et al. In vitro and in vivo studies on the degradation of high-purity Mg (99.99wt.%) screw with femoral intracondylar fractured rabbit model. *Biomaterials*. 2015;64:57–69.
15. Wu C, Chen Z, Wu Q, et al. Clinoenstatite coatings have high bonding strength, bioactive ion release, and osteoimmunomodulatory effects that enhance in vivo osseointegration. *Biomaterials*. 2015;71:35–47.

16. Yu H-J, Wang J-Q, Shi X-T, Louzguine-Luzgin DV, Wu H-K, Perepezko JH. Ductile biodegradable Mg-based metallic glasses with excellent biocompatibility. *Adv Funct Mater.* 2013;23:4793–4800.
17. Gu X, Zheng Y, Cheng Y, Zhong S, Xi T. In vitro corrosion and biocompatibility of binary magnesium alloys. *Biomaterials.* 2009;30(4):484–498.
18. Zhang X, Zhang C, Xu W, et al. Biodegradable mesoporous calcium–magnesium silicate-polybutylene succinate scaffolds for osseous tissue engineering. *Int J Nanomedicine.* 2015;10:6699–6708.
19. Wu Z, Zheng K, Zhang J, et al. Effects of magnesium silicate on mechanical property, biocompatibility, bioactivity, degradability, osteogenesis of poly(butylene succinate) based composite scaffolds for bone repair. *J Mater Chem B.* 2016;4:7974–7988.
20. Dai C, Yuan Y, Liu C, et al. Degradable, antibacterial silver exchanged mesoporous silica spheres for hemorrhage control. *Biomaterials.* 2009;30(29):5364–5375.
21. Rajesh R, Ravichandran YD. Development of a new carbon nanotube-alginate-hydroxyapatite tricomponent composite scaffold for application in bone tissue engineering. *Int J Nanomedicine.* 2015;10(suppl 1):7–15.
22. Cai Y, Guo L, Shen H, et al. Degradability, bioactivity, and osteogenesis of biocomposite scaffolds of lithium-containing mesoporous bioglass and mPEG-PLGA-b-PLL copolymer. *Int J Nanomedicine.* 2015;10:4125–4136.
23. Kim MH, Park WH. Chemically cross-linked silk fibroin hydrogel with enhanced elastic properties, biodegradability, and biocompatibility. *Int J Nanomedicine.* 2016;11:2967–2978.
24. Kokubo T, Takadama H. How useful is SBF in predicting in vivo bone bioactivity. *Biomaterials.* 2006;27(15):2907–2915.
25. Addison WN, Nelea V, Chicatun F, et al. Extracellular matrix mineralization in murine MC3T3-E1 osteoblast cultures: an ultrastructural, compositional and comparative analysis with mouse bone. *Bone.* 2015;71:244–256.
26. Zhang P, Han F, Li Y, et al. Local delivery of controlled-release simvastatin to improve the biocompatibility of polyethylene terephthalate artificial ligaments for reconstruction of the anterior cruciate ligament. *Int J Nanomedicine.* 2016;11:465–478.
27. Gu J, Liu J, Li Y, Zhao W, Shi J. One-pot synthesis of mesoporous silica nanocarriers with tunable particle sizes and pendent carboxylic groups for cisplatin delivery. *Langmuir.* 2012;29(1):403–410.
28. Wu S, Liu X, Yeung KWK, Liu C, Yang X. Biomimetic porous scaffolds for bone tissue engineering. *Mater Sci Eng R.* 2014;80:1–36.
29. Fu Q, Saiz E, Rahaman MN, Tomsia AP. Toward strong and tough glass and ceramic scaffolds for bone repair. *Adv Funct Mater.* 2013;23(44):5461–5476.
30. Afisco M, Sandri M, Panseri S, Delgado-López JM, Gómez-Morales J, Tampieri A. Magnetic bioactive and biodegradable hollow Fe-doped hydroxyapatite coated poly(l-lactic) acid micro-nanospheres. *Chem Mater.* 2013;25(13):2610–2617.
31. Zhou P, Cheng X, Xia Y, et al. Organic/inorganic composite membranes based on poly(L-lactic-co-glycolic acid) and mesoporous silica for effective bone tissue engineering. *ACS Appl Mater Interfaces.* 2014;6(23):20895–20903.
32. Zhang C, McAdams DA 2nd, Grunlan JC. Nano/micro-manufacturing of bioinspired materials: a review of methods to mimic natural structures. *Adv Mater.* 2016;28(30):6292–6321.
33. Parizek M, Douglas TE, Novotna K, et al. Nanofibrous poly(lactide-co-glycolide) membranes loaded with diamond nanoparticles as promising substrates for bone tissue engineering. *Int J Nanomedicine.* 2012;7:1931–1951.
34. Wang Z, Wu G, Wei M, et al. Improving the osteogenesis of human bone marrow mesenchymal stem cell sheets by microRNA-21-loaded chitosan/hyaluronic acid nanoparticles via reverse transfection. *Int J Nanomedicine.* 2016;11:2091–2105.
35. Rocca A, Marino A, Rocca V, et al. Barium titanate nanoparticles and hypergravity stimulation improve differentiation of mesenchymal stem cells into osteoblasts. *Int J Nanomedicine.* 2015;10:433–445.
36. Wu C, Chen Z, Yi D, Chang J, Xiao Y. Multidirectional effects of Sr-, Mg-, and Si-containing bioceramic coatings with high bonding strength on inflammation, osteoclastogenesis, and osteogenesis. *ACS Appl Mater Interfaces.* 2014;6(6):4264–4276.
37. Xie Z, Liu X, Jia W, Zhang C, Huang W, Wang J. Treatment of osteomyelitis and repair of bone defect by degradable bioactive borate glass releasing vancomycin. *J Control Release.* 2009;139(2):118–126.
38. Chou YC, Cheng YS, Hsu YH, Yu YH, Liu SJ. A bio-artificial poly([D,L]-lactide-co-glycolide) drug-eluting nanofibrous periosteum for segmental long bone open fractures with significant periosteal stripping injuries. *Int J Nanomedicine.* 2016;11:941–953.
39. Atefyekta S, Ercan B, Karlsson J, et al. Antimicrobial performance of mesoporous titania thin films: role of pore size, hydrophobicity, and antibiotic release. *Int J Nanomedicine.* 2016;11:977–990.

International Journal of Nanomedicine

Publish your work in this journal

The International Journal of Nanomedicine is an international, peer-reviewed journal focusing on the application of nanotechnology in diagnostics, therapeutics, and drug delivery systems throughout the biomedical field. This journal is indexed on PubMed Central, MedLine, CAS, SciSearch®, Current Contents®/Clinical Medicine,

Submit your manuscript here: <http://www.dovepress.com/international-journal-of-nanomedicine-journal>

Dovepress

Journal Citation Reports/Science Edition, EMBase, Scopus and the Elsevier Bibliographic databases. The manuscript management system is completely online and includes a very quick and fair peer-review system, which is all easy to use. Visit <http://www.dovepress.com/testimonials.php> to read real quotes from published authors.